ACS APPLIED MATERIALS & INTERFACES

www.acsami.org

Research Article

Wafer-Scale Two-Dimensional MoS_2 Layers Integrated on Cellulose Substrates Toward Environmentally Friendly Transient Electronic Devices

Changhyeon Yoo, Md Golam Kaium, Luis Hurtado, Hao Li, Sushant Rassay, Jinwoo Ma, Tae-Jun Ko, Sang Sub Han, Mashiyat Sumaiya Shawkat, Kyu Hwan Oh, Hee-Suk Chung, and Yeonwoong Jung*

Cite This: *ACS Appl. Mater. Interfaces* 2020, 12, 25200–25210

Read Online

ACCESS | Metrics & More | Article Recommendations | Supporting Information

ABSTRACT: We explored the feasibility of wafer-scale two-dimensional (2D) molybdenum disulfide (MoS_2) layers toward futuristic environmentally friendly electronics that adopt biodegradable substrates. Large-area (> a few cm^2) 2D MoS_2 layers grown on silicon dioxide/silicon (SiO_2/Si) wafers were delaminated and integrated onto a variety of cellulose-based substrates of various components and shapes in a controlled manner; examples of the substrates include planar papers, cylindrical natural rubbers, and 2,2,6,6-tetramethylpiperidine-1-oxyl-oxidized cellulose nanofibers. The integrated 2D layers were confirmed to well preserve their intrinsic structural and chemical integrity even on such exotic substrates. Proof-of-concept devices employing large-area 2D MoS_2 layers/cellulose substrates were demonstrated for a variety of applications, including photodetectors, pressure sensors, and field-effect transistors. Furthermore, we demonstrated the complete "dissolution" of the integrated 2D MoS_2 layers in a buffer solution composed of baking soda and deionized water, confirming their environmentally friendly transient characteristics. Moreover, the approaches to delaminate and integrate them do not demand any chemicals except for water, and their original substrates can be recycled for subsequent growths, ensuring excellent chemical benignity and process sustainability.

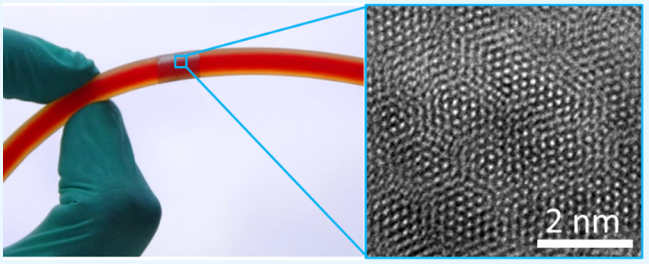

KEYWORDS: *2D TMD, 2D MoS_2 layer, transient electronics, paper electronics, cellulose substrate, water-assisted layer integration*

INTRODUCTION

Modern electronics have ubiquitously evolved, incorporating a diverse set of device functionalities and physical forms in a way to overcome the fundamental limitations of conventional technologies. For instance, consumer electronics such as cell phones or laptops have relied on a large number of device components that are nonrecyclable/perishable and potentially toxic (e.g., silicon wafers doped with chemically hazardous elements). As they are frequently upgraded, an overwhelming amount of "electronic wastes" are irreversibly discarded, which demands a substantial amount of landfill spaces, causing serious environmental threats.[1−3] To avoid environmental contamination and harmful effects on human health due to electronic wastes, substantial research efforts have been driven toward incorporating the following attributes in final device products: (1) replacement of conventional device materials with those that are intrinsically biodegradable and recyclable, and (2) development of device components that can naturally disintegrate in a biofriendly and environmentally benign manner beyond their intended functioning lifetime. The developing field of "transient electronics" endeavors to incorporate such transient features into device components, which, along with their underlying substrates, would completely dissolve after the targeted operation, releasing only environmentally benign end products at controllable rates.[4−7] These "green" approaches not only can significantly mitigate the excessive landfill issues but also can offer unprecedented functionalities unattainable with any other technologies; for instance, storage devices that can self-disassemble after predefined time sets, preventing unauthorized access and achieving improved data security,[7,8] or medical devices that can dissolve in physiological conditions with complete resorption, avoiding secondary surgeries for device retrieval.[9,10] Some proof-of-concept works have investigated electronic devices composed of biodegradable components as well as their environmentally friendly disintegration, demonstrating applications including integrated circuits, sensors, and supercapacitors.[4,11−13] For active device components, biodegradable polymers have been mainly adopted in earlier

Received: April 3, 2020
Accepted: May 13, 2020
Published: May 13, 2020

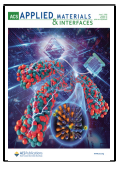

https://dx.doi.org/10.1021/acsami.0c06198
ACS Appl. Mater. Interfaces 2020, 12, 25200–25210

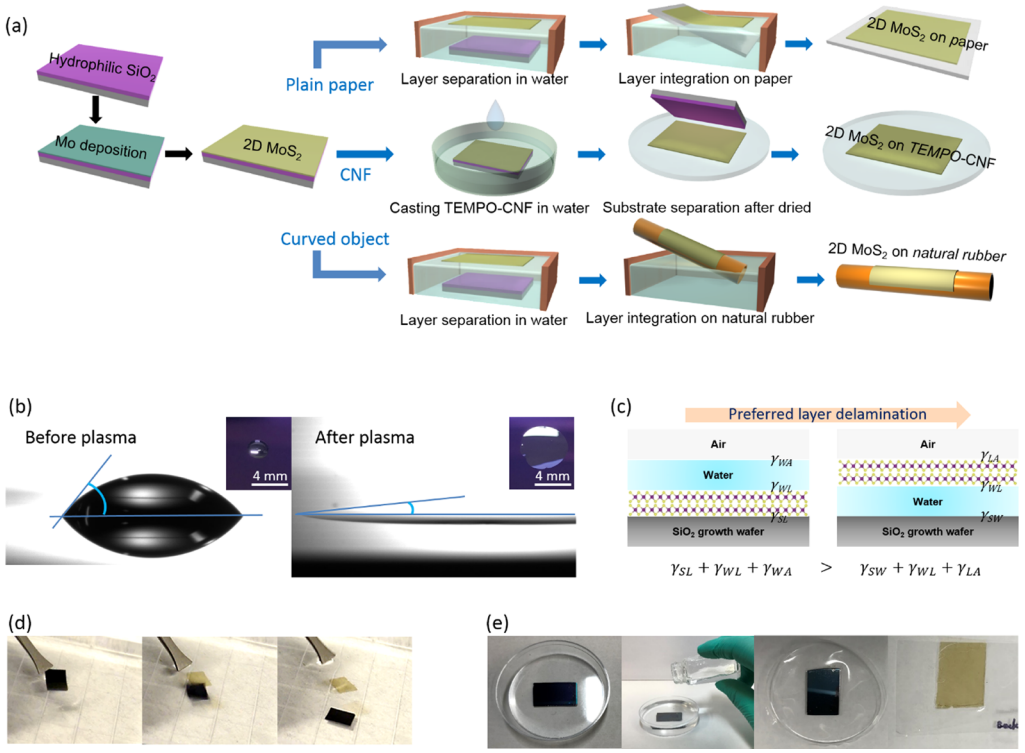

Figure 1. Water-assisted transfer and integration of 2D MoS_2 layers onto various biodegradable substrates. (a) Schematic illustrations for delamination and integration of 2D MoS_2 layers on plain papers (top), TOCNs (middle), and curved natural rubbers (bottom). (b) Water contact angle measurements to verify the conversion of hydrophilicity to superhydrophilicity in the SiO_2 surface via plasma treatment. (c) Schematic illustrations of the thermodynamic requirement for the delamination of 2D layers in water. (d) Time-span snapshots of water-assisted unprompted delamination of 2D MoS_2 layers from a SiO_2/Si substrate. (e) Images to describe the sequential procedure of delaminating 2D MoS_2 layers from the SiO_2/Si substrate and integrating them onto a TOCN substrate.

works,[12−14] while their electrical properties (e.g., carrier mobility and conductivity) are intrinsically limited for high-performance applications. Amongst inorganic semiconductors, such as nanomembranes of monocrystalline silicon (Si NMs) and thin films of zinc oxide (ZnO), have been adopted, owing to their intrinsic biocompatibility and environmental benignity,[4,15,16] while their mechanical brittleness poses a major concern for expanding their application range. With the transient electronics technology still at its initial phase, the widening search for alternative materials that can satisfy the demanded transient features with bio/environmental benignity as well as suitable electrical/mechanical properties is highly timely.[5,6,17] Near-atom thickness transition metal dichalcogenide (TMD) layers have recently received extensive attention for a wide range of unprecedented device technologies due to their unparalleled optoelectrical properties coupled with excellent mechanical flexibility.[18−21] However, utilizing them as active components for environmentally friendly devices and characterizing their intrinsic transient characteristics have remained largely unexplored. In addition to active device components, identifying suitable substrate materials that intrinsically possess desired biocompatibility and environmental compatibility is essential. Cellulose is one of the most abundant natural polymers—i.e., ∼1.5 trillion tons of the total annual biomass production—which is renewable, biocompatible, and biodegradable.[22−24] Green devices employing celluloses derived from woods have received extensive attention for applications requiring cost efficiency and mechanical deformability as well as environmental sustainability.[22,23,25,26] Examples include paper-based lithium-ion batteries (LIBs),[27] microwave and digital electronics fabricated on cellulose nanofibril papers,[26] and strain sensors based on transparent wood-derived thin films.[28] Especially, cellulose nanofibers (CNFs)—a special form of biosubstance chemically or mechanically extracted from cellulose—exhibit numerous advantages, such as high stiffness, transparency, and surface area, low density, thermal expansion coefficient, and excellent thermal stability.[23,25,26,29,30]

In this report, we explored the feasibility of 2D TMD layers for environmentally friendly transient electronics by using 2D molybdenum disulfide (MoS_2) layers as a representative example. Specifically, we grew wafer-scale 2D MoS_2 layers with a typical lateral dimension of ∼10 cm × 2 cm[31−34] on top of "superhydrophilic" silicon dioxide/silicon (SiO_2/Si) substrates. Then, we delaminated them inside water by taking advantage of their surface energy contrast against their growth substrates. We then integrated them on a variety of biodegradable substrates, such as plain papers, natural rubber, and highly transparent and flexible 2,2,6,6-tetramethylpiperidine-1-oxyl (TEMPO)-oxidized cellulose nanofibers (TOCNs). A variety of proof-of-concept devices were demonstrated utilizing the integrated 2D MoS_2 layers, including mechanically flexible photodetectors, pressure sensors, and field-effect transistors (FETs). In addition to achieving the targeted device functionality, we also demonstrated the controlled disintegration of 2D MoS_2 layers in an environmentally benign manner, confirming their intrinsic transient characteristics. We completely dissolved the integrated 2D MoS_2 layers in a biocompatible buffer solution based on a baking soda and identified their conversion to

https://dx.doi.org/10.1021/acsami.0c06198
ACS Appl. Mater. Interfaces 2020, 12, 25200−25210

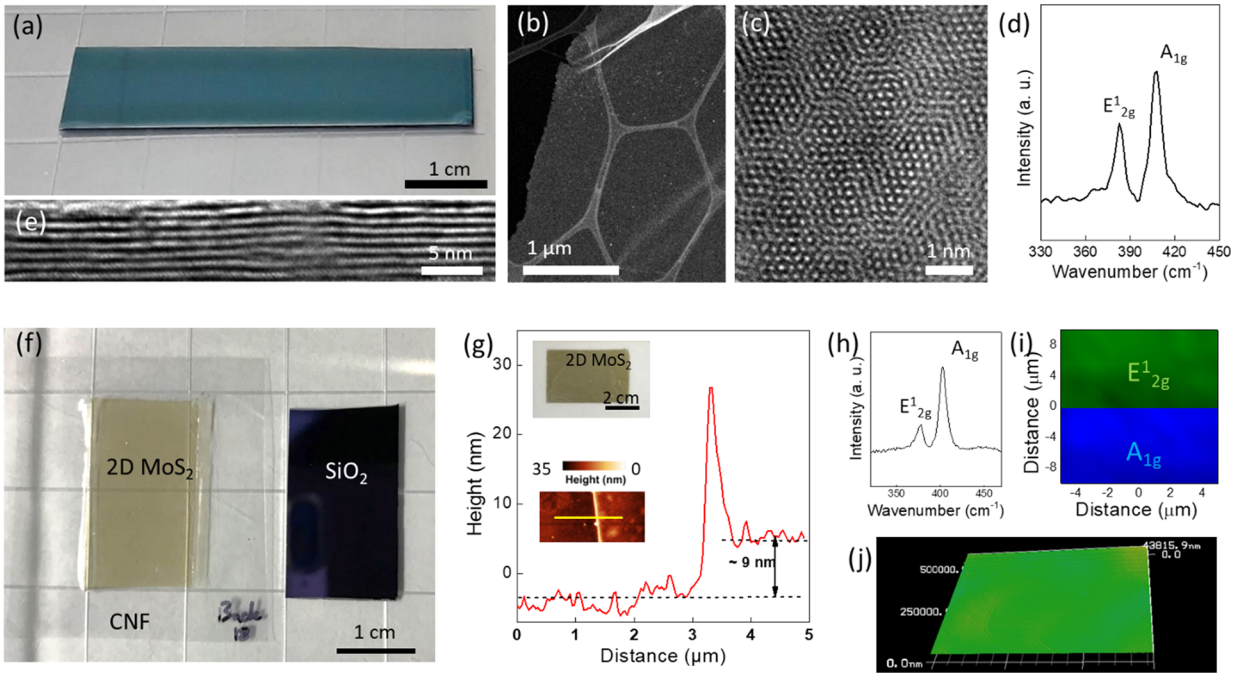

Figure 2. Characterization of 2D MoS_2 layers integrated on cellulose-based substrates. (a) Optical image of centimeter-scale 2D MoS_2 layers grown on a SiO_2/Si substrate. (b) Low-magnification plane-view TEM and (c) corresponding HRTEM image of 2D MoS_2 multilayers. (d) Raman spectrum obtained from as-grown 2D MoS_2 layers on a SiO_2/Si substrate. (e) Cross-sectional HRTEM image of 2D MoS_2 multilayers. (f) Optical image of 2D MoS_2 layers integrated on a TOCN substrate (left) and the original SiO_2/Si substrate after their delamination (right). (g) Optical image of 2D MoS_2 layers integrated on a glossy paper (top inset) and the corresponding AFM topography image (height profile) of their edge on the paper (bottom inset). The main plot presents the thickness measurement of the 2D MoS_2 layers corresponding to the AFM image in the inset. (h) Raman spectrum obtained from the sample in panel (g). (i) Raman mapping images corresponding to the characteristic peaks in panel (h). (j) Confocal microscopy characterization of the sample corresponding to panels (g)−(i).

molybdenum oxide (MoO_x), which is a nontoxic and environmentally friendly chemical. This study suggests that near-atom thickness wafer-scale 2D MoS_2 layers and their water-assisted integration approaches enable highly promising building blocks toward futuristic environmentally friendly electronic technologies.

RESULTS AND DISCUSSIONS

Inspired by the transient electronics, we envisioned and fabricated 2D MoS_2 layers on biodegradable substrates by employing biofriendly green methods that involve only water for their transfers and integrations. Figure 1a shows the illustrations of integrating wafer-scale 2D MoS_2 layers on three representative examples of biodegradable substrates: (1) 2D plain papers, (2) optically transparent TOCNs, and (3) 3D curved objects. The integrations start with the chemical vapor deposition (CVD) growth of 2D MoS_2 layers on surface-treated SiO_2/Si growth substrates via a thermal sulfurization of Mo thin films. Bare SiO_2/Si substrates are first treated with argon (Ar) plasma, which leads to "superhydrophilic" surfaces—to be verified in the next section. Then, Mo films of controlled thickness are deposited on the superhydrophilic SiO_2/Si wafers followed by the CVD sulfurization, which converts them to 2D MoS_2 layers. Then, the prepared samples are immersed in water for the delamination of 2D MoS_2 layers, which becomes facilitated by the superhydrophilicity of SiO_2/Si surfaces. For the integrations of 2D MoS_2 layers onto plain papers (top) and curved rubbers (bottom), the 2D layers are spontaneously separated from the growth substrates and manually scooped by the target substrates.[32] For the integration of 2D MoS_2 layers onto TOCNs (middle), separately prepared TOCN dispersions (gels) mixed with deionized (DI) water are directly solution-casted onto 2D MoS_2-grown SiO_2/Si substrates. After drying at room temperature, the TOCN-casted 2D MoS_2 layers are manually peeled off from the growth substrates. Note that TOCNs have recently drawn increasing attention as device substrates due to their biocompatibility along with excellent visible light transparency (~90%), mechanical flexibility, and bendability.[25,29,30,35] Details for the preparation of TOCNs are presented in the Methods section. It is worth mentioning that conventional methods for transferring and integrating 2D MoS_2 layers involve polymeric adhesive layers as well as chemical reagents to etch away the underlying substrates. Evidently, 2D MoS_2 layers can be exposed to the strong, hazardous chemicals, which can potentially deteriorate their material properties,[36,37] or can be fragmented upon removing the polymer layers by additionally applied chemicals (e.g., acetone).[38] The processes schematically described in Figure 1a are entirely green as they only involve water without any other chemicals to delaminate, transfer, and integrate centimeter-scale 2D MoS_2 layers onto virtually arbitrary substrates of any kinds and shapes. We have previously observed the facile delamination of 2D MoS_2 layers immersed in water,[32] which is attributed to maximizing the surface energy contrast between as-grown 2D layers versus underlying SiO_2/Si substrates. While this water-assisted delamination method generally applies to any growth substrates, its efficacy is delicately dependent on the surface quality of the substrates and grown 2D layers as it is determined by their surface energy imbalance. Given the intrinsic hydrophobicity of 2D layers, a large amount of energy contrast should result against them as far as the surface of the

https://dx.doi.org/10.1021/acsami.0c06198
ACS Appl. Mater. Interfaces 2020, 12, 25200−25210

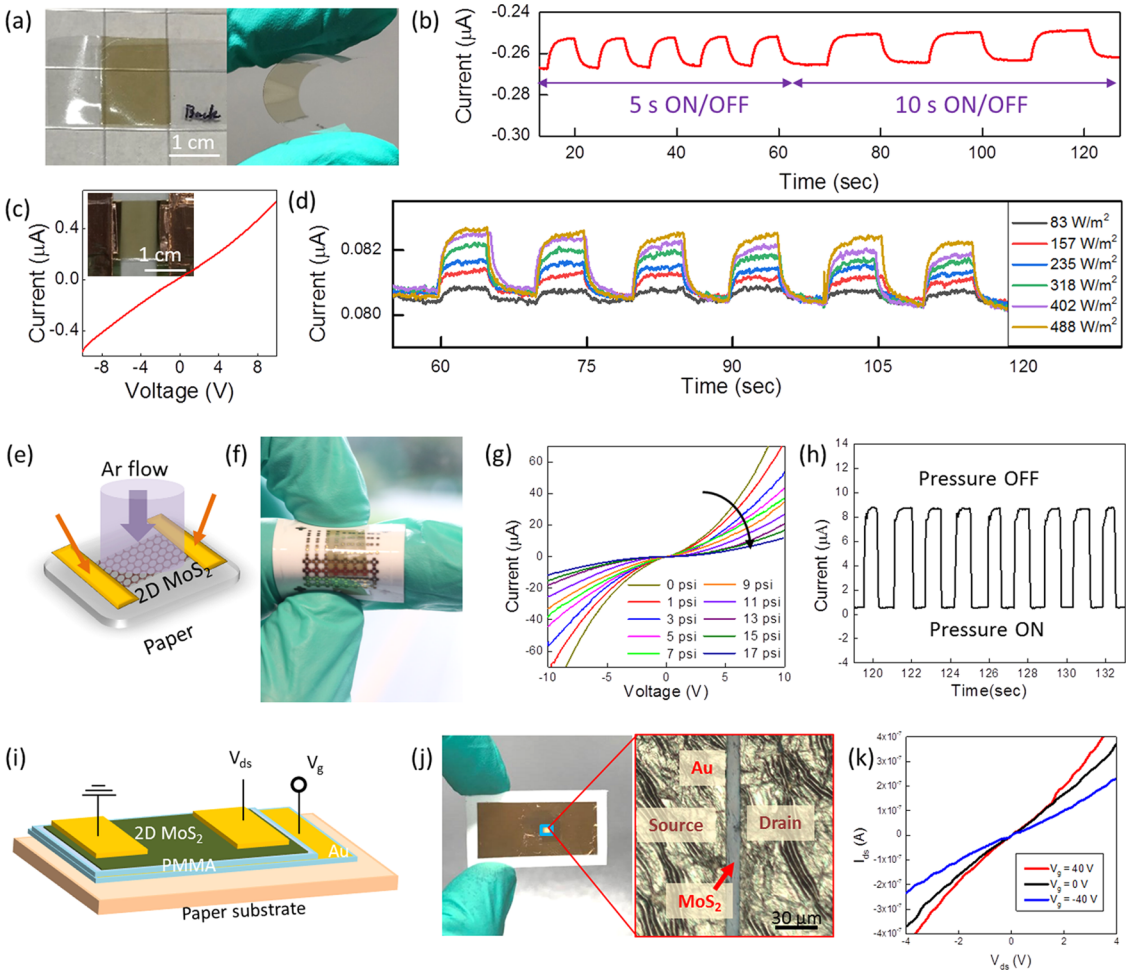

Figure 3. Demonstrations of proof-of-concept devices utilizing 2D MoS_2 layers integrated on cellulose substrates. (a)−(d) Photodetectors based on 2D MoS_2 layers integrated on TOCN substrates. (a) Images of the 2D MoS_2 layer-integrated TOCN paper (left) and its mechanical bending (right). (b) Time-dependent photoresponsiveness from the sample in panel (a). (c) *I*−*V* characteristics from the sample in the inset. (d) Time-dependent photoresponsiveness with varying light intensity obtained from the sample in panel (c). (e)−(h) Pressure sensors based on 2D MoS_2 layers integrated on planar paper substrates. (e) Schematic illustration of pressure sensing. (f) Image of 2D MoS_2 layers integrated on a flexible paper with an array of Au top electrodes. (g) *I*−*V* characteristics obtained from varying pressure levels. (h) Time−current characteristics under a periodic application of constant Ar pressure. (i)−(k) FETs based on 2D MoS_2 layers integrated on paper substrates; (i) Schematic illustration of a FET employing 2D MoS_2 layers integrated on a PMMA/Au/PMMA/Paper. (j) Optical image of a FET and its magnified view visualizing device components. (k) I_{ds}−V_{ds} output characteristics obtained with varying V_g.

growth wafers becomes more hydrophilic. This enlarged surface energy contrast facilitates the delamination of 2D layers off their growth substrates upon immersion in water—to be explained in the next section. Accordingly, it is desirable to develop an approach that can "actively" control the surface properties of growth substrates, which will greatly improve the efficacy of 2D layer delamination and transfer. We identified a transition of the surface energy of a SiO_2/Si wafer before/after the plasma treatment by measuring its water wettability, as presented in the optical microscopy images of water contact angles in Figure 1b. The images reveal that the initially moderate hydrophilicity of a SiO_2/Si wafer manifested by the water contact angle of >50° (left) transits to super-hydrophilicity, i.e., a water contact angle of <10°, after the plasma treatment (right). The inset images present top-down views of water droplets for each case. Plasma-driven surface modifications of SiO_2/Si wafers to increase hydrophilicity have been well established in the literature,[39−41] while their underlying mechanisms vary with types of employed plasmas, e.g., alteration of surface charge density or surface roughness.

Figure 1c illustrates the two distinct situations that the water-assisted delamination of 2D layers is not preferred (left) versus preferred (right) considering the following thermodynamic energy requirements: (1) Total interfacial energies should become smaller if the delamination is to occur (thus, is preferred), i.e., $\gamma_{SL} + \gamma_{WL} + \gamma_{WA}$ (left) > $\gamma_{SW} + \gamma_{WL} + \gamma_{LA}$(right) where W, A, L, and S represent water, air, 2D layers, and growth substrate, respectively. (2) The penetration of water in between the 2D layers and the underlying growth wafers should be exerted by a positive amount of driving force, i.e., work of adhesion, $W_{ad} = \gamma_{SW} + \gamma_{WL} - \gamma_{SL} > 0$. In a way to maximize the driving force, it is imperative to maximize the water/substrate interfacial energy (γ_{SW}), which indicates the increased surface wettability (Figure 1b, right). Figure 1d shows time span-sequential snapshots demonstrating the unprompted delamination of 2D MoS_2 layers from a SiO_2/Si substrate assisted by water. Freestanding 2D MoS_2 layers maintaining their original shapes and sizes float on the water surface and are ready for subsequent transfer and integration onto any target substrates. Figure 1e shows the sequence of

https://dx.doi.org/10.1021/acsami.0c06198
ACS Appl. Mater. Interfaces 2020, 12, 25200−25210

integrating 2D MoS_2 layers on a TOCN paper substrate by the above-described solution-casting method. Once the TOCN solution cast onto the surface of 2D MoS_2 layers−SiO_2/Si substrate is dried at room temperature for >48 h, the Petri dish is removed, and then, the dried 2D MoS_2 layers/TOCN paper is manually peeled off from the wafer substrate.

Before exploring the device applications of 2D MoS_2 layers integrated on biodegradable paper and TOCN substrates, we first characterize their structural and chemical integrity before and after the integration. Cellulose papers are recently gaining interest as alternative device substrates, owing to their high mechanical flexibility, high thermal budget, and environmental benignity, while TOCNs are particularly promising for optoelectronic applications, owing to their intrinsic optical transparency.[6,23,25,29,30,35] Figure 2a shows an optical image of as-grown centimeter-scale 2D MoS_2 layers on a SiO_2/Si substrate. Figure 2b presents a low-magnification plane-view transmission electron microscopy (TEM) image of 2D MoS_2 layers delaminated from their growth substrates, revealing their continuous film morphology. Figure 2c shows the corresponding high-resolution TEM (HRTEM) plane-view image, unveiling the atomic-scale Moiré fringes of hexagonal 2D MoS_2 multilayers. Figure 2d shows a Raman spectroscopy profile obtained from the sample in Figure 2a, confirming the presence of in-plane (E^1_{2g}) and out-of-plane (A_{1g}) vibration modes inherent to 2D MoS_2 multilayers.[32,42,43] Figure 2e is a cross-sectional TEM image of the 2D MoS_2 multilayers, revealing horizontally aligned and well-resolved individual 2D layers of uniform interlayer spacing. Figure 2f shows images of 2D MoS_2 layers integrated on a transparent TOCN substrate (left) and the original SiO_2/Si substrate used for their growth (right). The images show that the integrated 2D MoS_2 layers well replicate the original shape/dimension of the growth substrate, confirming the excellent fidelity of the water-assisted TOCN delamination method. The Figure 2g inset shows an image of 2D MoS_2 layers integrated on a piece of glossy paper, and the main plot presents an atomic force microscopy (AFM) height profile obtained from the 2D MoS_2/paper interface, corresponding to the bottom inset AFM image. The results confirm ∼9 nm-thick 2D MoS_2 layers obtained by the CVD sulfurization of ∼3 nm Mo films, which is consistent with our previous studies and others.[31,34] We further characterized the material quality of 2D MoS_2 layers integrated on these biodegradable substrates by Raman spectroscopy. Figure 2h shows a Raman spectrum corresponding to the sample in Figure 2g, revealing the characteristic E^1_{2g} and A_{1g} peaks of 2D MoS_2 layers. The peak positions are consistent with those obtained from the as-grown 2D MoS_2 layers on SiO_2/Si substrates (Figure 2d) before their delamination and integration. Figure 2i shows Raman mapping images corresponding to Figure 2h, conducted on the same sample area where the E^1_{2g} (green) and A_{1g} (blue) peaks were obtained. The uniform colors in Figure 2i indicate the high spatial homogeneity of 2D MoS_2 layers integrated on the paper substrate, confirming that their intrinsic structural characteristics are well preserved even after the delamination. In furtherance of confirming the structural uniformity of the integrated 2D MoS_2 layers, we performed confocal microscopy characterization on the sample corresponding to Figure 2g. The confocal microscopy image in Figure 2j indicates high spatial homogeneity and surface smoothness, as revealed by the uniform color distribution over a large area of ∼1 cm^2. All these comprehensive characterization results confirm that the 2D MoS_2 layers integrated on the biodegradable paper and TOCN substrates well maintain the excellent structural and chemical integrity inherent to their as-grown substrates.

Having confirmed the material quality of 2D MoS_2 layers integrated on cellulose-based substrates, we set on pursuing their electronic device applications. We demonstrate a variety of proof-of-concept devices to verify the generality and versatility of this integration approach, i.e., applications in photo-detection, pressure sensing, and field-effect transistor (FET). Figure 3a−d presents photodetection applications of 2D MoS_2 layers integrated on TOCN substrates. Figure 3a shows camera images of 2D MoS_2 layers integrated on a TOCN substrate (left), which become subsequently deformed (right), confirming the excellent optical transparency and mechanical bendability of the sample. Figure 3b shows the time-dependent photoresponsiveness of the corresponding sample manifested by its current change upon a periodically applied optical illumination. A white light-emitting diode (LED, with an intensity of ∼164 W/m^2) was turned on/off on top of the sample, causing the increase/decrease of the current, respectively, at intervals of 5 and 10 s. Figure 3c shows the two-terminal electrical characterization of another 2D MoS_2 layers/TOCN sample (inset), revealing its current−voltage (I−V) characteristics with gold (Au) electrodes in contact. Figure 3d shows the photoresponsiveness of the sample in Figure 3c under the illumination of a collimated LED (THORLABS; with a wavelength of 625 nm) with varying light intensities. The results confirm that the device exhibits excellent time- and intensity-dependent photosensitivity, confirming the 2D MoS_2 layers integrated on the TOCN substrate well retain their intrinsic semiconducting properties. Figure 3e−h presents pressure-sensing applications of 2D MoS_2 layers integrated on glossy paper substrates. Figure 3e shows a schematic illustration of a two-terminal 2D MoS_2 layers/paper device for pressure sensing, depicting that Ar gas of controlled pressure levels is applied onto the active sensing media, i.e., 2D MoS_2 layers, through a quarter-inch tubing. Figure 3f shows optical images of 2D MoS_2 layers integrated on a paper substrate with an array of Au electrodes patterned on the surface. The sample contains a large number of individual device units, presenting excellent mechanical adaptability and flexibility. Figure 3g shows representative I−V characteristics obtained from the device, revealing a systematic decrease in the current under increasing pressure levels. It is noted that the device well responds to a large degree of pressure change (from 0 to 17 psi), which is attributed to the elastic nature of both 2D MoS_2 layers and paper substrates. Figure 3h shows the pressure-induced current responses from a device under a periodic Ar pressure application of 0 and 4 psi, confirming its high reversible sensitivity. Figure 3i−k presents FET applications of 2D MoS_2 layers integrated on paper substrates. Figure 3i shows a schematic illustration of the FET device structure along with its measurement configuration. The device employs 2D MoS_2 layers as the channel, Au electrodes as the top source/drain and back-gate contacts, and polymethyl methacrylate (PMMA) as the dielectric layer.[44] Before the integration of 2D MoS_2 layers, a paper substrate is first coated with PMMA to improve the adhesion of the Au gate, which is directly deposited on it. Subsequently, another layer of thin (∼500 nm) PMMA is deposited on top of the Au gate, which functions as the dielectric. Then, 2D MoS_2 layers are integrated onto the PMMA dielectric via the water-assisted integration method

https://dx.doi.org/10.1021/acsami.0c06198
ACS Appl. Mater. Interfaces 2020, 12, 25200−25210

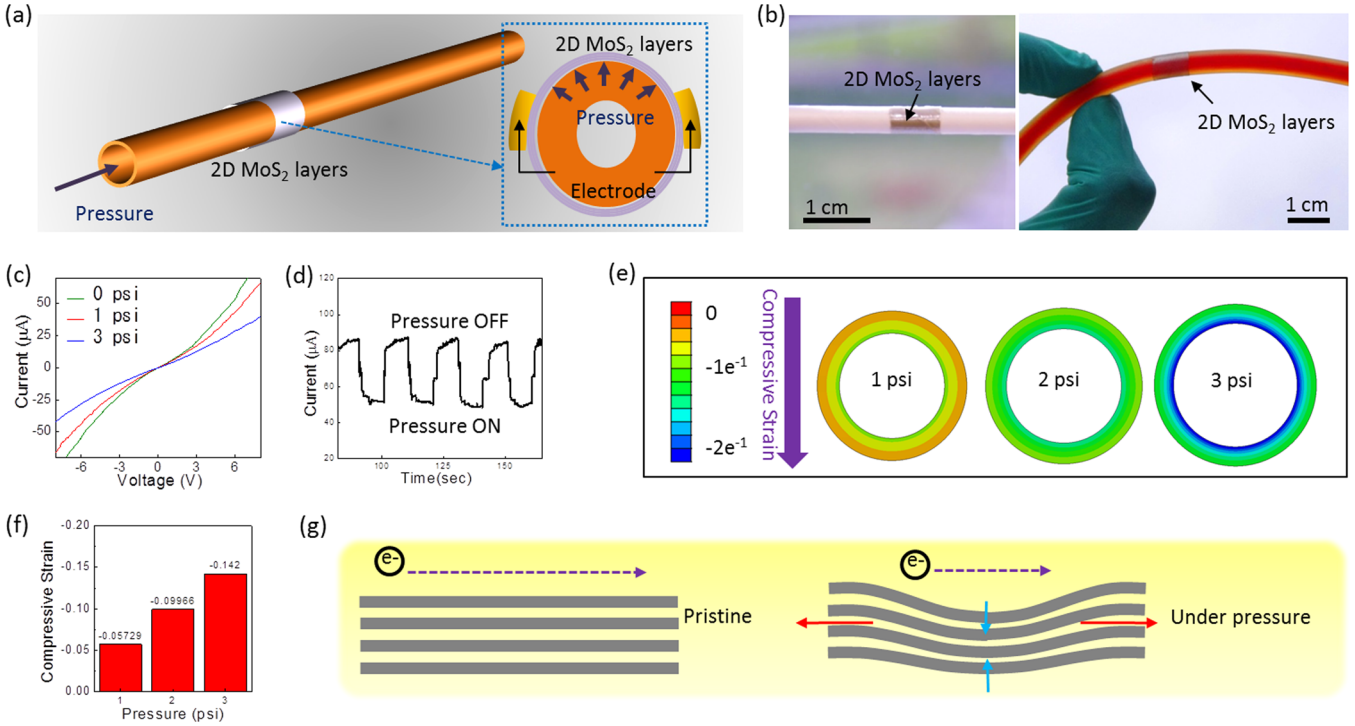

Figure 4. Demonstration of pressure sensing using 2D MoS_2 layers integrated on a cylindrical natural rubber vessel. (a) Schematic illustration of 2D MoS_2 layers integrated on an artificial blood vessel. (b) Optical images of 2D MoS_2 layers integrated on a paper straw (left) and a rubber vessel (right). (c) I-V characteristics with varying pressure levels. (d) Time−current characteristics under a periodic application of Ar pressure. (e) FEM calculations revealing the spatial distribution of strain developed within the circumference of a natural rubber vessel. (f) Plot of compressive strain versus applied pressure corresponding to panel (e). (g) Schematic illustrations of electron transports within 2D MoS_2 layers in a pristine state (left) and under a vertically applied pressure (right) presented in a side view.

followed by the deposition of Au source/drain electrodes. Figure 3j shows an image of a fabricated FET device employing large-area 2D MoS_2 layers integrated on a paper substrate. The enlarged image corresponding to the device area (blue square) reveals that the 2D MoS_2 layers (channel length, ~12 μm) are in contact with Au source/drain electrodes. Figure 3k shows drain-source current versus voltage (I_{ds}−V_{ds}) output characteristics obtained at three different gate voltages (V_g) of −40, 0, and 40 V. The results confirm that I_{ds} increases with increasing V_g, indicating the n-type semiconducting transport of 2D MoS_2 layers.

Having demonstrated the device applications of 2D MoS_2 layers integrated on planar cellulose substrates as presented in Figure 3, we further extended to integrating 2D MoS_2 layers on three-dimensionally curved objects for increased versatility. We envisioned to simulate a potential application of 2D MoS_2 layers for sensing blood pressure exerted onto the circumference of a blood vessel in the arterial walls of living animals. Mechanical responses of blood vessels are mainly determined by passive components such as elastin and collagen whose viscoelastic/plastoelastic properties have been extensively studied.[45,46] Figure 4a shows a schematic illustration that simulates the pressure-sensing model of 2D MoS_2 layers integrated on the circumference of an artificial blood vessel. As pressure flows through the vessel in the longitudinal direction, the vessel will radially expand, exerting tensile stress to its circumference. This circumferential tension will, in turn, exert compressive strain onto the 2D MoS_2 layers preattached to its side wall, leading to a change of electrical response, similar to the pressure sensing demonstrated in Figure 3e−h. Figure 4b shows the integration of 2D MoS_2 layers on highly curved objects, achieved by the method described in Figure 1a, i.e., integration onto a cellulose paper straw and a biodegradable natural rubber latex artificial blood vessel,[47] respectively. Considering their very similar mechanical properties to human arteries,[45] we demonstrated the electrical pressure sensing of 2D MoS_2 layers integrated onto natural rubber vessels in a way to project their potential for blood pressure sensing. Figure 4c shows I−V characteristics obtained from 2D MoS_2 layers attached to a natural rubber vessel through which Ar gas of various pressure levels is exerted. Figure 4d presents the dynamics of current versus time under a periodic application of 3 psi of Ar gas flowing through the vessel, which further confirms the decreasing current with the increasing pressure. To better understand the origin of the pressure-induced current decrease, we employed a finite element method (FEM) and simulated the spatial distribution of stress distribution within the artificial vessel exerted by varying pressures. Figure 4e visualizes the cross-sectional view of compressive stress exerted within the radial circumference of a vessel corresponding to the cross-sectional schematic in Figure 4a. With increasing pressure levels, compressive strain steadily increases in the radial direction, which is normal to the 2D MoS_2 layers attached to the vessel. The observation indicates that the rigidly integrated 2D MoS_2 layers on the periphery of the vessel simultaneously experience both compressive and tensile strains along their out-of-plane and in-plane direction, respectively. Figure 4f presents a quantification of the compressive strain that the 2D MoS_2 layers on the vessel experience under varying pressure levels, obtained from FEM calculations. Figure 4g is a schematic presentation of electron transports within 2D MoS_2 layers without (left)

https://dx.doi.org/10.1021/acsami.0c06198
ACS Appl. Mater. Interfaces 2020, 12, 25200−25210

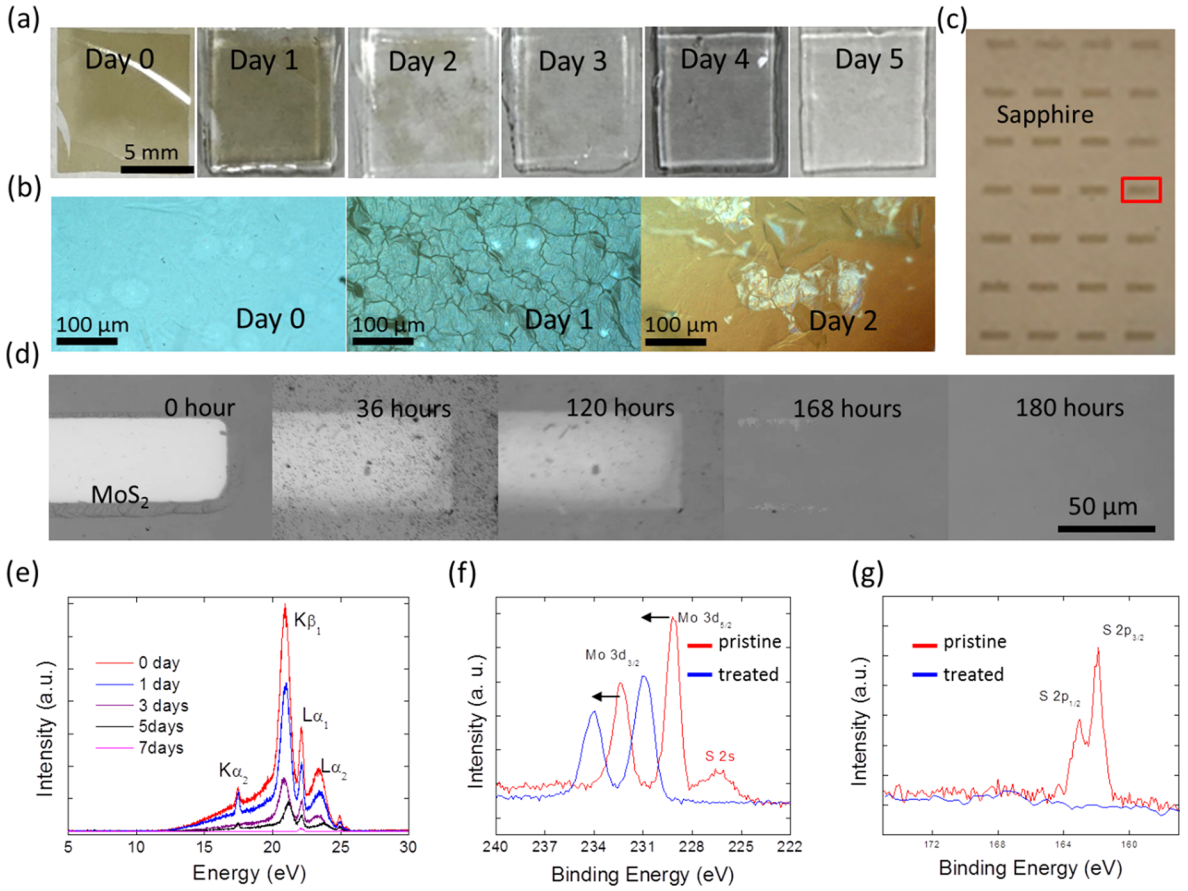

Figure 5. Biodegradable dissolution of 2D MoS_2 layers using the BSB solution. (a) Optical images revealing the time-lapse dissolution of 2D MoS_2 layers integrated on a TOCN substrate. (b) Enlarged views of the disintegrating 2D MoS_2 layers corresponding to panel (a). (c) Optical image of an array of patterned 2D MoS_2 layers grown on a sapphire substrate. (d) Optical images revealing the time-lapse dissolution of 2D MoS_2 layers corresponding to the red box in panel (c). (e)XRF characterization of 2D MoS_2 layers under dissolution for various time periods. (f), (g) XPS spectra of (f) Mo 3d and S 2s and (g) S 2p core levels before (red plots) and after (blue plots) treatment with the BSB solution.

and with (right) applied pressure in a side view. In the pristine state (no pressure), electrons can travel along 2D MoS_2 layers between electrodes with minimum interruptions. When pressure is externally applied in an orthogonal orientation with respect to their basal planes (Figures 3e and 4a), both compressive (blue arrows) and tensile (red arrows) strains will be exerted through them in the vertical and horizontal orientations, respectively. This mechanical force will lead to their elastic deformation, which will cause an increase in resistance $R=\rho\frac{l}{A}$ where ρ is the resistivity, l is the distance between electrodes, and A is the cross-sectional area, respectively. The cause of the pressure-induced resistance increase must be a combined effect of reduced cross-sectional area A and pronounced scattering of electrons within deformed 2D layers. This analysis can be generalized to account for the electrical measurement results obtained from 2D MoS_2 layers integrated on planar papers without curvature (Figure 3e–h) and cylindrical natural rubbers (Figure 4).

After the successful demonstrations of targeted device functionalities from 2D MoS_2 layers integrated on biodegradable papers, TOCNs, and natural rubber substrates, we attempted to demonstrate their feasibility as transient electronics, i.e., electronic devices completely dissolve and disappear once completing their designated tasks, which ideally should happen in a biofriendly manner. Considering that 2D MoS_2 layers are water insoluble[48] and highly stable under ambient conditions,[49−51] we targeted to disassemble 2D MoS_2 layers in biofriendly buffer solutions.[52,53] We prepared for a buffer solution by mixing a commercially available pure baking soda composed of sodium bicarbonate ($NaHCO_3$) with DI water. Details for the preparation of the buffer solution are presented in the Methods section. Historically, $NaHCO_3$ has been used for biorelated applications in mummification,[54] antibacterial agents,[55] and lactic acidosis treatment,[56] owing to its intrinsic biocompatibility. $NaHCO_3$ dissociates into Na^+ and H_2CO_3, and the resulting Na^+ can intercalate through the van der Waals (vdW) gaps of 2D MoS_2 layers,[57,58] which eventually can break up Mo−S atomic bonds, forming sodium sulfide (Na_2S) and molybdenum trioxide (MoO_3).[53,59] Formation of Na_2S and MoO_3 can further enhance the dissolution rate of 2D MoS_2 layers, generating structural misfit, stress, and vacancies in them.[60] We first studied the dissolution kinetics of 2D MoS_2 layers integrated on TOCN substrates inside the baking soda buffer (BSB) solution. Figure 5a shows the time-lapse images of 2D MoS_2 layers integrated on a TOCN substrate in the BSB solution set at 75 °C with pH ~9.04 for 6 days. The images clearly reveal that 2D MoS_2 layers become steadily disintegrated with increasing time, resulting in their complete removal in ~5 days. The concentration (50 mL of 0.1 M) of the BSB solution was well maintained throughout the entire time frame. Figure 5b shows optical microscope images, revealing the enlarged views

https://dx.doi.org/10.1021/acsami.0c06198
ACS Appl. Mater. Interfaces 2020, 12, 25200−25210

of progressively disassembling 2D MoS_2 layers on a TOCN substrate in the BSB solution. It is obvious that cracks form after ~24 h, and they serve as the starting points of chemical reactions, which slowly extend toward the outer regions, indicating defect-accelerated degradation.[53,61] In order to rule out any potential influences of the TOCN substrate on dissolution efficacy, we also directly grew 2D MoS_2 layers on other substrates (e.g., sapphire substrates; Figure 5c) and studied their dissolution kinetics in the BSB solution. Figure 5d shows time-lapse snapshot images of 2D MoS_2 layers corresponding to the red box in Figure 5c under prolonged exposure to the BSB solution. The progressively fading image contrast of 2D MoS_2 layers with respect to the almost identical background contrast reveals time-dependent dissolution, which was completed after ~180 h. In addition to the BSB solution, we also demonstrated the dissolution of 2D MoS_2 layers in a commercially available phosphate-buffered saline (PBS) solution, which is also biofriendly. Corresponding images are presented in the Supporting Information, Figure S1. We note that both BSB and PBS solutions contain Na^+ ions, which are known to distort the lattice of 2D MoS_2 layers via the formation of Na_2S which eventually becomes converted to soluble NaS_2.[53,58,62] Increasing their concentration is anticipated to accelerate the degradation kinetics of 2D MoS_2.[53,58,63,64] For the quantification of dissolution kinetics, we performed the X-ray fluorescence (XRF) characterization of 2D MoS_2 layers undergoing dissolution for varying time periods. Figure 5e shows XRF profiles obtained from 2D MoS_2 layers dissolved for up to 7 days, which reveals a decreasing peak intensity with increasing dissolution times. We also employed X-ray photoelectron spectroscopy (XPS) to clarify the dissolution chemistry of 2D MoS_2 layers before/after dissolved in buffer solutions (BSB solution, in this case) by characterizing their oxidation states. Figure 5f compares the XPS spectra of Mo 3d and S 2s core levels obtained from a sample of 2D MoS_2 layers in its pristine state and after treatment with the BSB solution for 8 days. In the pristine state (red plot), the observed XPS peaks correspond to Mo $3d_{5/2}$ (229.1 eV), Mo $3d_{3/2}$ (232.3 eV), and S 2s (226.3 eV),[65] indicating the atomic ratio of stoichiometric 2D MoS_2 layers. Once the 2D MoS_2 layers are treated with the BSB solution (blue plot), XPS peaks exhibit a noticeable shift, indicating a change in the oxidation states of constituent elements; XPS peaks of Mo 3d core levels are observed at 231.0 and 234.1 eV, indicating a stoichiometric change from the Mo(IV) to Mo(V) oxidation state. Figure 5g compares the XPS spectra of S 2p core levels from the same sample before (red) and after (blue) the BSB solution treatment. The two characteristic peaks in the red plot observed at S $2p_{3/2}$ (161.9 eV) and S $2p_{1/2}$ (163.2 eV) indicate pristine sulfide (S^{2-}) present in stoichiometric 2D MoS_2 layers, which disappear upon the treatment as shown in the blue plot. The oxidation reaction of MoS_2 and $NaHCO_3$ projects a formation of molybdenum trioxide (MoO_3), i.e., Mo(VI) oxidation. At the same time, the XPS spectra in Figure 5f suggest a formation of Mo(V) instead of Mo(VI). This discrepancy is attributed to that MoO_3 is unstable in the hydroxide (OH^{-1})-rich buffer solution, which thus follows the reduction reaction pathway leading to lower oxidation states, as also verified in previous studies.[66] Nevertheless, this XPS characterization clearly confirms that the BSB solution converts MoS_2 to MoO_x, which is well known to be biofriendly.[53,61] All spectra have been referenced to a Au ($4f_{7/2}$) binding energy of 84.0 eV and compared with previous references and National Institute of Standards and Technology photoelectron database.[67−69] Reaction details for the dissolution of 2D MoS_2 layers in the BSB and the PBS solutions are presented in the Supporting Information, Figure S2. Lastly, we have also demonstrated the progressive dissolution of 2D MoS_2 layers integrated on paper substrates and present the results in the Supporting Information, Figure S3. In addition to dissolving 2D MoS_2 layers, we note that noble metals such as Au are dissolvable in the buffer solutions, which can release chloride ions.[70] In order to test the feasibility of the transient characteristics of Au electrodes integrated on 2D MoS_2 layers, we have prepared for another buffer solution by mixing up commercially available bleach and vinegar. We observed that the entire device components of Au/2D MoS_2 layers become completely dissolved in the solution within ~90 s, as presented in the Supporting Information, Figure S3b. As this bleach-based solution is chemically toxic, developing a biofriendly buffer solution, which can "universally" dissolve both 2D MoS_2 layers and other device components including metal electrodes in a biofriendly manner, needs to be pursued in the future.

CONCLUSIONS

In summary, we report device functionalities of wafer-scale 2D MoS_2 layers integrated on biodegradable substances, including planar paper and TOCN substrates, as well as cylindrical natural rubbers. 2D MoS_2 layers grown on superhydrophilic SiO_2/Si wafers were verified to be easily delaminated in water, owing to their significantly enlarged energy contrast against the wafers. The entire procedures to integrate the delaminated 2D MoS_2 layers onto secondary biodegradable substrates are chemically benign, rendering high environmental sustainability. A variety of proof-of-concept devices, including photodetectors, pressure sensors, and FETs, were demonstrated, verifying the versatility and reliability of this integration approach. Furthermore, we confirmed that 2D MoS_2 layers could be completely dissolved in biofriendly buffer solutions releasing nontoxic MoO_x, which indicates excellent implications for transient electronics. This study unveils the high promise of 2D TMDs toward futuristic transient electronic devices, which can function within programmed lifetimes and perform in an environmentally sustainable manner without producing electronic wastes.

METHODS

CVD Growth of Centimeter-Scale 2D MoS2 Layers. SiO_2 (300 nm thickness)/Si substrates were cleaned by ultrasonication in acetone, isopropyl alcohol (IPA), and DI water to remove any organic impurities. Mo (~3−4 nm thicknesses) were deposited on the substrates by e-beam evaporator (Thermionics VE-100) at a deposition rate of ~0.10−0.12 Å/s and at a chamber base pressure of 5.5×10^{-7} Torr. The Mo-deposited substrates were kept at the center of the CVD furnace chamber (Lindberg/Blue M Mini-Mite) along with sulfur (S) powder (≥99.5%, Sigma-Aldrich) placed on an alumina boat at the upstream side. The CVD chamber was pumped down to 25 mTorr, and ultrapure Ar gas was supplied at a flow rate of 100 sccm (standard cubic centimeter per minute). Subsequently, the CVD furnace was heated up to 800 °C in ~50 min and was maintained at the temperature for another ~50 min followed by natural cooling to room temperature.

Plasma Treatment. Prior to the Mo deposition for CVD growths, as-cleaned SiO_2/Si substrates were placed inside a plasma chamber (Harrick Plasma, model PDC-32G). Following initial evacuation down to ~10 mTorr, Ar gas of 10 psi pressure was purged into the chamber at a rate of 20 mL/min, achieving the desired chamber pressure of ~200 mTorr by a gas flow controller (Plasmaflo PDC-

https://dx.doi.org/10.1021/acsami.0c06198
ACS Appl. Mater. Interfaces 2020, 12, 25200−25210

FMG). Then, oxygen (O_2) or Ar plasma was activated, and the power of the chamber was maintained at 11 W for controlled duration times.

Water-Assisted Integration of 2D MoS_2 Layers on Papers and Natural Rubbers. CVD-2D MoS_2 layers on SiO_2/Si substrates are immersed in water until only 2D MoS_2 layers become spontaneously delaminated. The 2D MoS_2 layers floating on the water surface are then manually scooped and transferred to target substrates. The 2D MoS_2 layers integrated on papers and natural rubbers are dried in air at room temperature for few days or on hot plates at 70 °C for ∼12 h to ensure complete removal of residual water molecules. For the pressure-sensing measurements, 2D MoS_2 layers were integrated on commercially available glossy papers (Canon Pro Platinum, 0.30 mm in thickness) and artificial blood vessels (3B Scientific).

Solution-Casting Integration of 2D MoS_2 Layers on TOCN Substrates. Commercially available slurry (aqueous gel) TOCNs (CELLULOSELAB, width of ∼50 nm, lengths of approximately up to several hundred micrometers) in water (1 wt %) are mixed with DI water. Their diluted solution (0.5 wt %) is directly poured onto as-grown 2D MoS_2 layers on SiO_2/Si substrates and is dried at room temperature for more than 48 h until it turns to a transparent paper. After the drying stage, 2D MoS_2 layers integrated on the TOCN paper are manually peeled off from their growth substrates.

Materials Characterization. Raman spectral characterization, including Raman mapping, was performed with Nanofinder 30 Raman Confocal spectroscopy (Tokyo Instrument Inc.) using a laser source with a wavelength of 532 nm and a spot size of 1 μm. Confocal microscopy characterization was carried out with a VK-X100K scanning confocal microscope (Keyence). AFM (nanoIR2, Anasys Instruments) characterization was performed using Anasys AFM probe tips (PR-EX-T125−10) with a nominal spring constant of 30 N/m in a tapping mode at a scan rate of 1 Hz. XRF characterization of 2D MoS_2 layers dissolution was performed with Epsilon 1, Malvern Panalytical. XPS characterization was performed with a Thermo Scientific ESCALAB250Xi photoelectron spectrometer using an Al anode as the X-ray source (1486.68 eV). High-resolution spectra were obtained with 50 scans and 0.1 eV step size from a spot size of 650 μm under ultrahigh vacuum (10^{-9} mbar). TEM characterization was performed with Cs-corrected JEOL ARM 200F at an acceleration voltage of 200 kV. Cross-sectional TEM samples were prepared by focused ion beam (FIB)-based milling and lift-out techniques.

Electrical Measurements. For the pressure sensing measurements, Ar gas of precisely defined pressure levels was exerted through a quarter-inch vacuum tube controlled by a gas flow meter. For the photoresponsiveness measurements, a white LED (HS-72 LED) was used for the time-dependent photocurrent measurement and a 625 nm LED (M625L4-C2) was used for the time- and intensity-dependent photocurrent measurement. All photocurrent and electrical measurements were performed using a home-built probe station connected to a semiconductor parameter analyzer (HP 4156A).

Biodegradable Dissolution of 2D MoS_2 Layers. The BSB solution (concentration: 0.1 M) was prepared by dissolving commercially available baking soda (Arm & Hammer Pure Baking Soda) containing $NaHCO_3$ (0.84 g) in DI water (totaled to 100 mL). For the dissolution experiment of 2D MoS_2 layers on sapphire substrates, arrays of Mo (1 nm) films were deposited through a shadow mask (150 × 50 μm pattern size) followed by the identical CVD reaction adopted for SiO_2/Si substrates. For the XPS characterization, 2D MoS_2 layers were mixed with the BSB solution, and the liquid sample mixture was dispersed onto carbon tapes and followed by drying at room temperature.

■ ASSOCIATED CONTENT

Supporting Information

The Supporting Information is available free of charge at https://pubs.acs.org/doi/10.1021/acsami.0c06198.

Optical images for the dissolution of 2D MoS_2 layers integrated on TOCN and paper substrates, and reaction formula for the dissolution of 2D MoS_2 layers in BSB and PBS solutions (PDF)

■ AUTHOR INFORMATION

Corresponding Author

Yeonwoong Jung − *NanoScience Technology Center, Department of Materials Science and Engineering, and Department of Electrical and Computer Engineering, University of Central Florida, Orlando, Florida 32826, United States;* orcid.org/0000-0001-6042-5551; Email: Yeonwoong.Jung@ucf.edu

Authors

Changhyeon Yoo − *NanoScience Technology Center, University of Central Florida, Orlando, Florida 32826, United States*

Md Golam Kaium − *NanoScience Technology Center, University of Central Florida, Orlando, Florida 32826, United States*

Luis Hurtado − *NanoScience Technology Center, University of Central Florida, Orlando, Florida 32826, United States*

Hao Li − *NanoScience Technology Center and Department of Materials Science and Engineering, University of Central Florida, Orlando, Florida 32826, United States*

Sushant Rassay − *NanoScience Technology Center, University of Central Florida, Orlando, Florida 32826, United States*

Jinwoo Ma − *Department of Materials Science and Engineering, Seoul National University, Seoul 08826, South Korea*

Tae-Jun Ko − *NanoScience Technology Center, University of Central Florida, Orlando, Florida 32826, United States*

Sang Sub Han − *NanoScience Technology Center, University of Central Florida, Orlando, Florida 32826, United States; Department of Materials Science and Engineering, Seoul National University, Seoul 08826, South Korea*

Mashiyat Sumaiya Shawkat − *NanoScience Technology Center and Department of Electrical and Computer Engineering, University of Central Florida, Orlando, Florida 32826, United States;* orcid.org/0000-0001-6594-190X

Kyu Hwan Oh − *Department of Materials Science and Engineering, Seoul National University, Seoul 08826, South Korea*

Hee-Suk Chung − *Analytical Research Division, Korea Basic Science Institute, Jeonju 54907, South Korea*

Complete contact information is available at: https://pubs.acs.org/10.1021/acsami.0c06198

Author Contributions

C.Y. and M.G.K. equally contributed to the work. Y.J. conceived the project and directed it. C.Y. and M.G.K. performed a majority of the sample preparation and pressure sensing measurement assisted by S.R. and M.S.S. They also performed the dissolution experiment and characterization. L.H. performed the FET device fabrication and measurement. H.L. performed the AFM characterization. T.-J.K, and S.S. H. assisted the sample preparation. J.M. performed the FEM simulation under the guidance of K.H.O. H.-S.C. performed the TEM and Raman characterization. C.Y., M.G.K., L.H., and H.L. wrote the manuscript with inputs from all authors.

Notes

The authors declare no competing financial interest.

https://dx.doi.org/10.1021/acsami.0c06198
ACS Appl. Mater. Interfaces 2020, 12, 25200−25210

■ ACKNOWLEDGMENTS

Y.J. acknowledges financial supports from the National Science Foundation (CMMI-1728390), the Korea Institute of Energy Technology Evaluation and Planning (KETEP), the Ministry of Trade, Industry and Energy (MOTIE) of the Republic of Korea (no. 20173010013340), and the VPR Advancement of Early Career Researchers award from the University of Central Florida.

■ REFERENCES

(1) Robinson, B. H. E-waste: An Assessment of Global Production and Environmental Impacts. *Sci. Total Environ.* **2009**, *408*, 183−191.
(2) Geyer, R.; Blass, V. D. The Economics of Cell Phone Reuse and Recycling. *Int. J. Adv. Manuf. Technol.* **2010**, *47*, 515−525.
(3) Kumar, U.; Singh, D. Electronic waste: Concerns & Hazardous Threats. *Int. J. Curr. Eng. Technol* **2014**, *47*, 802−525.
(4) Hwang, S.-W.; Tao, H.; Kim, D.-H.; Cheng, H.; Song, J.-K.; Rill, E.; Brenckle, M. A.; Panilaitis, B.; Won, S. M.; Kim, Y.-S.; Song, Y. M.; Yu, K. J.; Ameen, A.; Li, R.; Su, Y.; Yang, M.; Kaplan, D. L.; Zakin, M. R.; Slepian, M. J.; Huang, Y.; Omenetto, F. G.; Rogers, J. A. A Physically Transient Form of Silicon Electronics. *Science* **2012**, *337*, 1640−1644.
(5) Fu, K. K.; Wang, Z.; Dai, J.; Carter, M.; Hu, L. Transient Electronics: Materials and Devices. *Chem. Mater.* **2016**, *28*, 3527−3539.
(6) Li, R.; Wang, L.; Kong, D.; Yin, L. Recent Progress on Biodegradable Materials and Transient Electronics. *Bioact. Mater.* **2018**, *3*, 322−333.
(7) Lei, T.; Guan, M.; Liu, J.; Lin, H.-C.; Pfattner, R.; Shaw, L.; McGuire, A. F.; Huang, T.-C.; Shao, L.; Cheng, K.-T.; Tok, J. B.-H.; Bao, Z. Biocompatible and Totally Disintegrable Semiconducting Polymer for Ultrathin and Ultralightweight Transient Electronics. *Proc. Natl. Acad. Sci. U. S. A.* **2017**, *114*, 5107−5112.
(8) Tanskanen, P. Management and Recycling of Electronic Waste. *Acta Mater.* **2013**, *61*, 1001−1011.
(9) Irimia-Vladu, M.; Troshin, P. A.; Reisinger, M.; Shmygleva, L.; Kanbur, Y.; Schwabegger, G.; Bodea, M.; Schwödiauer, R.; Mumyatov, A.; Fergus, J. W.; Razumov, V. F.; Sitter, H.; Sacriciftci, N. S.; Bauer, S. Biocompatible and Biodegradable Materials for Organic Field-Effect Transistors. *Adv. Funct. Mater.* **2010**, *20*, 4069−4076.
(10) Tao, H.; Hwang, S.-W.; Marelli, B.; An, B.; Moreau, J. E.; Yang, M.; Brenckle, M. A.; Kim, S.; Kaplan, D. L.; Rogers, J. A.; Omenetto, F. G. Silk-Based Resorbable Electronic Devices for Remotely Controlled Therapy and in Vivo Infection Abatement. *Proc. Natl. Acad. Sci. U. S. A.* **2014**, *111*, 17385−17389.
(11) Salvatore, G. A.; Sülzle, J.; Dalla Valle, F.; Cantarella, G.; Robotti, F.; Jokic, P.; Knobelspies, S.; Daus, A.; Büthe, L.; Petti, L.; Kirchgessner, N.; Hopf, R.; Magno, M.; Tröster, G. Biodegradable and Highly Deformable Temperature Sensors for the Internet of Things. *Adv. Funct. Mater.* **2017**, *27*, 1702390.
(12) Hwang, S.-W.; Lee, C. H.; Cheng, H.; Jeong, J.-W.; Kang, S.-K.; Kim, J.-H.; Shin, J.; Yang, J.; Liu, Z.; Ameer, G. A.; Huang, Y.; Rogers, J. A. Biodegradable Elastomers and Silicon Nanomembranes/Nanoribbons for Stretchable, Transient Electronics, and Biosensors. *Nano Lett.* **2015**, *15*, 2801−2808.
(13) Kang, S.-K.; Murphy, R. K.; Hwang, S.-W.; Lee, S. M.; Harburg, D. V.; Krueger, N. A.; Shin, J.; Gamble, P.; Cheng, H.; Yu, S.; Liu, Z.; McCall, J. G.; Stephen, M.; Ying, H.; Kim, J.; Park, G.; Webb, R. C.; Lee, C. H.; Chung, S.; Wie, D. S.; Gujar, A. D.; Vemulapalli, B.; Kim, A. H.; Lee, K.-M.; Cheng, J.; Huang, Y.; Lee, S. H.; Braun, P. V.; Ray, W. Z.; Rogers, J. A. Bioresorbable Silicon Electronic Sensors for the Brain. *Nature* **2016**, *530*, 71.
(14) Armentano, I.; Dottori, M.; Fortunati, E.; Mattioli, S.; Kenny, J. M. Biodegradable Polymer Matrix Nanocomposites for Tissue Engineering: a Review. *Polym. Degrad. Stab.* **2010**, *95*, 2126−2146.
(15) Yin, L.; Farimani, A. B.; Min, K.; Vishal, N.; Lam, J.; Lee, Y. K.; Aluru, N. R.; Rogers, J. A. Mechanisms for Hydrolysis of Silicon Nanomembranes as Used in Bioresorbable Electronics. *Adv. Mater.* **2015**, *27*, 1857−1864.
(16) Dagdeviren, C.; Hwang, S.-W.; Su, Y.; Kim, S.; Cheng, H.; Gur, O.; Haney, R.; Omenetto, F. G.; Huang, Y.; Rogers, J. A. Transient, Biocompatible Electronics and Energy Harvesters Based on ZnO. *Small* **2013**, *9*, 3398−3404.
(17) Cheng, H.; Vepachedu, V. Recent Development of Transient Electronics. *Theor. Appl. Mech. Lett.* **2016**, *6*, 21−31.
(18) Wang, M.; Li, H.; Ko, T.-J.; Sumaiya Shawkat, M.; Okogbue, E.; Yoo, C.; Han, S. S.; Islam, M. A.; Oh, K. H.; Jung, Y. Manufacturing Strategies for Wafer-Scale Two-Dimensional Transition Metal Dichalcogenide Heterolayers. *J. Mater. Res.* **2020**, 1−19.
(19) Mak, K. F.; Lee, C.; Hone, J.; Shan, J.; Heinz, T. F. Atomically Thin MoS_2: A New Direct-Gap Semiconductor. *Phys. Rev. Lett.* **2010**, *105*, 136805.
(20) Yoshida, M.; Suzuki, R.; Zhang, Y.; Nakano, M.; Iwasa, Y. Memristive Phase Switching in Two-Dimensional 1T-TaS_2 crystals. *Science Advances* **2015**, *1*, No. e1500606.
(21) Tan, C.; Cao, X.; Wu, X.-J.; He, Q.; Yang, J.; Zhang, X.; Chen, J.; Zhao, W.; Han, S.; Nam, G.-H.; Sindoro, M.; Zhang, H. Recent Advances in Ultrathin Two-Dimensional Nanomaterials. *Chem. Rev.* **2017**, *117*, 6225−6331.
(22) Moon, R. J.; Martini, A.; Nairn, J.; Simonsen, J.; Youngblood, J. Cellulose Nanomaterials Review: Structure, Properties and Nanocomposites. *Chem. Soc. Rev.* **2011**, *40*, 3941−3994.
(23) Eichhorn, S. J. Cellulose Nanowhiskers: Promising Materials for Advanced Applications. *Soft Matter* **2011**, *7*, 303−315.
(24) Kim, J.-H.; Shim, B. S.; Kim, H. S.; Lee, Y.-J.; Min, S.-K.; Jang, D.; Abas, Z.; Kim, J. Review of Nanocellulose for Sustainable Future Materials. *Int. J. Pt. Eng. Man.-GT* **2015**, *2*, 197−213.
(25) Saito, T.; Kimura, S.; Nishiyama, Y.; Isogai, A. Cellulose Nanofibers Prepared by TEMPO-Mediated Oxidation of Native Cellulose. *Biomacromolecules* **2007**, *8*, 2485−2491.
(26) Jung, Y. H.; Chang, T.-H.; Zhang, H.; Yao, C.; Zheng, Q.; Yang, V. W.; Mi, H.; Kim, M.; Cho, S. J.; Park, D.-W.; Jiang, H.; Lee, J.; Qiu, Y.; Zhou, W.; Cai, Z.; Gong, S.; Ma, Z. High-Performance Green Flexible Electronics based on Biodegradable Cellulose Nanofibril Paper. *Nat. Commun.* **2015**, *6*, 7170.
(27) Hu, L.; Wu, H.; La Mantia, F.; Yang, Y.; Cui, Y. Thin, Flexible Secondary Li-Ion Paper Batteries. *ACS Nano* **2010**, *4*, 5843−5848.
(28) Fu, Q.; Chen, Y.; Sorieul, M. Wood-Based Flexible Electronics. *ACS Nano* **2020**, 3528.
(29) Isogai, A.; Saito, T.; Fukuzumi, H. TEMPO-Oxidized Cellulose Nanofibers. *Nanoscale* **2011**, *3*, 71−85.
(30) Yang, W.; Jiao, L.; Liu, W.; Dai, H. Manufacture of Highly Transparent and Hazy Cellulose Nanofibril Films via Coating TEMPO-Oxidized Wood Fibers. *Nanomaterials* **2019**, *9*, 107.
(31) Choudhary, N.; Chung, H. S.; Kim, J. H.; Noh, C.; Islam, M. A.; Oh, K. H.; Coffey, K.; Jung, Y.; Jung, Y. Strain-Driven and Layer-Number-Dependent Crossover of Growth Mode in van der Waals Heterostructures: 2D/2D Layer-By-Layer Horizontal Epitaxy to 2D/3D Vertical Reorientation. *Adv. Mater. Interfaces* **2018**, 1800382.
(32) Kim, J. H.; Ko, T.-J.; Okogbue, E.; Han, S. S.; Shawkat, M. S.; Kaium, M. G.; Oh, K. H.; Chung, H.-S.; Jung, Y. Centimeter-Scale Green Integration of Layer-by-Layer 2D TMD vdW Heterostructures on Arbitrary Substrates by Water-Assisted Layer Transfer. *Sci. Rep.* **2019**, *9*, 1641.
(33) Kong, D.; Wang, H.; Cha, J. J.; Pasta, M.; Koski, K. J.; Yao, J.; Cui, Y. Synthesis of MoS_2 and $MoSe_2$ Films with Vertically Aligned Layers. *Nano Lett.* **2013**, *13*, 1341−1347.
(34) Jung, Y.; Shen, J.; Liu, Y.; Woods, J. M.; Sun, Y.; Cha, J. J. Metal Seed Layer Thickness-Induced Transition From Vertical to Horizontal Growth of MoS_2 and WS_2. *Nano Lett.* **2014**, *14*, 6842−6849.
(35) Fukui, S.; Ito, T.; Saito, T.; Noguchi, T.; Isogai, A. Surface-Hydrophobized TEMPO-Nanocellulose/Rubber Composite Films Prepared in Heterogeneous and Homogeneous Systems. *Cellulose* **2019**, *26*, 463−473.

https://dx.doi.org/10.1021/acsami.0c06198
ACS Appl. Mater. Interfaces 2020, 12, 25200−25210

(36) Bertolazzi, S.; Brivio, J.; Kis, A. Stretching and Breaking of Ultrathin MoS_2. *ACS Nano* **2011**, *5*, 9703−9709.
(37) Li, Y.; Li, A.; Li, F.; Liu, D.; Chai, Y.; Liu, C. Application of HF Etching in a HRTEM Study of Supported MoS_2 Catalysts. *J. Catal.* **2014**, *317*, 240−252.
(38) Lin, Y.-C.; Zhang, W.; Huang, J.-K.; Liu, K.-K.; Lee, Y.-H.; Liang, C.-T.; Chu, C.-W.; Li, L.-J. Wafer-Scale MoS_2 Thin Layers Prepared by MoO_3 Sulfurization. *Nanoscale* **2012**, *4*, 6637−6641.
(39) Suni, T.; Henttinen, K.; Suni, I.; Mäkinen, J. Effects of Plasma Activation on Hydrophilic Bonding of Si and SiO_2. *J. Electrochem. Soc.* **2002**, *149*, G348.
(40) Cong, C.; Li, K.; Zhang, X. X.; Yu, T. Visualization of Arrangements of Carbon Atoms in Graphene Layers by Raman Mapping and Atomic-Resolution TEM. *Sci. Rep.* **2013**, *3*, 1195.
(41) Alam, A. U.; Howlader, M. M. R.; Deen, M. J. The Effects of Oxygen Plasma and Humidity on Surface Roughness, Water Contact Angle and Hardness of Silicon, Silicon Dioxide and Glass. *J. Micromech. Microeng.* **2014**, *24*, No. 035010.
(42) Li, H.; Zhang, Q.; Yap, C. C. R.; Tay, B. K.; Edwin, T. H. T.; Olivier, A.; Baillargeat, D. From Bulk to Monolayer MoS_2: Evolution of Raman Scattering. *Adv. Funct. Mater.* **2012**, *22*, 1385−1390.
(43) Verble, J. L.; Wietling, T. J.; Reed, P. R. Rigid-Layer Lattice Vibrations and van der Waals Bonding in Hexagonal MoS_2. *Solid State Commun.* **1972**, *11*, 941−944.
(44) Bao, W.; Cai, X.; Kim, D.; Sridhara, K.; Fuhrer, M. S. High Mobility Ambipolar MoS_2 Field-Effect Transistors: Substrate and Dielectric Effects. *Appl. Phys. Lett.* **2013**, *102*, No. 042104.
(45) Dobrin, P. B. Mechanical Properties of Arteries. *Physiol. Rev.* **1978**, *58*, 397−460.
(46) Monson, K. L.; Goldsmith, W.; Barbaro, N. M.; Manley, G. T. Axial Mechanical Properties of Fresh Human Cerebral Blood Vessels. *J. Biomech. Eng.* **2003**, *125*, 288−294.
(47) Rose, K.; Steinbüchel, A. Biodegradation of Natural Rubber and Related Compounds: Recent Insights into a Hardly Understood Catabolic Capability of Microorganisms. *Appl. Environ. Microbiol.* **2005**, *71*, 2803.
(48) Haynes, W. M. *CRC Handbook of Chemistry and Physics*; CRC Press: 2014.
(49) Kc, S.; Longo, R. C.; Wallace, R. M.; Cho, K. Surface Oxidation Energetics and Kinetics on MoS_2 Monolayer. *J. Appl. Phys.* **2015**, *117*, 135301.
(50) Mirabelli, G.; McGeough, C.; Schmidt, M.; McCarthy, E. K.; Monaghan, S.; Povey, I. M.; McCarthy, M.; Gity, F.; Nagle, R.; Hughes, G.; Cafolla, A.; Hurley, P. K.; Duffy, R. Air Sensitivity of MoS_2, $MoSe_2$, $MoTe_2$, HfS_2, and $HfSe_2$. *J. Appl. Phys.* **2016**, *120*, 125102.
(51) Longo, R. C.; Addou, R.; Santosh, K. C.; Noh, J.-Y.; Smyth, C. M.; Barrera, D.; Zhang, C.; Hsu, J. W. P.; Wallace, R. M.; Cho, K. Intrinsic Air Stability Mechanisms of Two-Dimensional Transition Metal Dichalcogenide Surfaces: Basal versus Edge Oxidation. *2D Mater.* **2017**, *4*, 025050.
(52) Aracena, A.; Rubilar, R.; Jerez, O.; Carvajal, D. Dissolution of MoS_2 Concentrate Using NaClO from 283 to 373 K. *Can. Metall. Q.* **2016**, *54*, 455−459.
(53) Chen, X.; Park, Y. J.; Kang, M.; Kang, S.-K.; Koo, J.; Shinde, S. M.; Shin, J.; Jeon, S.; Park, G.; Yan, Y.; MacEwan, M. R.; Ray, W. Z.; Lee, K.-M.; Rogers, J. A.; Ahn, J.-H. CVD-Grown Monolayer MoS_2 in Bioabsorbable Electronics and Biosensors. *Nat. Commun.* **2018**, *9*, 1690.
(54) Lucas, A. The Use of Natron by the Ancient Egyptians in Mummification. *J. Egypt. Archaeol.* **1914**, *1*, 119−123.
(55) Corral, L. G.; Post, L. S.; Montville, T. J. Antimicrobial Activity of Sodium Bicarbonate. *J. Food Sci.* **1988**, *53*, 981−982.
(56) Forsythe, S. M.; Schmidt, G. A. Sodium Bicarbonate for the Treatment of Lactic Acidosis. *Chest* **2000**, *117*, 260−267.
(57) Zhang, J.; Yang, A.; Wu, X.; van de Groep, J.; Tang, P.; Li, S.; Liu, B.; Shi, F.; Wan, J.; Li, Q.; Sun, Y.; Lu, Z.; Zheng, X.; Zhou, G.; Wu, C.-L.; Zhang, S.-C.; Brongersma, M. L.; Li, J.; Cui, Y. Reversible and Selective ion Intercalation Through the Top Surface of Few-Layer MoS_2. *Nat. Commun.* **2018**, *9*, 5289.
(58) Wang, X.; Shen, X.; Wang, Z.; Yu, R.; Chen, L. Atomic-Scale Clarification of Structural Transition of MoS_2 upon Sodium Intercalation. *ACS Nano* **2014**, *8*, 11394−11400.
(59) González, J. R.; Alcántara, R.; Tirado, J. L.; Fielding, A. J.; Dryfe, R. A. W. Electrochemical Interaction of Few-Layer Molybdenum Disulfide Composites vs Sodium: New Insights on the Reaction Mechanism. *Chem. Mater.* **2017**, *29*, 5886−5895.
(60) Martincová, J.; Otyepka, M.; Lazar, P. Is Single Layer MoS_2 Stable in the Air. *Chem. − Eur. J.* **2017**, *23*, 13233−13239.
(61) Chen, X.; Shinde, S. M.; Dhakal, K. P.; Lee, S. W.; Kim, H.; Lee, Z.; Ahn, J.-H. Degradation Behaviors and Mechanisms of MoS_2 Crystals Relevant to Bioabsorbable Electronics. *NPG Asia Mater.* **2018**, *10*, 810−820.
(62) Zhang, L.; Tang, Y.; Wang, Y.; Duan, Y.; Xie, D.; Wu, C.; Cui, L.; Li, Y.; Ning, X.; Shan, Z. In Situ TEM Observing Structural Transitions of MoS_2 upon Sodium Insertion and Extraction. *RSC Adv.* **2016**, *6*, 96035−96038.
(63) Dungey, K. E.; Curtis, M. D.; Penner-Hahn, J. E. Structural Characterization and Thermal Stability of MoS_2 Intercalation Compounds. *Chem. Mater.* **1998**, *10*, 2152−2161.
(64) Wang, L.; Xu, Z.; Wang, W.; Bai, X. Atomic Mechanism of Dynamic Electrochemical Lithiation Processes of MoS_2 Nanosheets. *J. Am. Chem. Soc.* **2014**, *136*, 6693−6697.
(65) Ganta, D.; Sinha, S.; Haasch, R. T. 2-D Material Molybdenum Disulfide Analyzed by XPS. *Surf. Sci. Spectra* **2014**, *21*, 19−27.
(66) Wang, Z.; Zhu, W.; Qiu, Y.; Yi, X.; von dem Bussche, A.; Kane, A.; Gao, H.; Koski, K.; Hurt, R. Biological and Environmental Interactions of Emerging Two-Dimensional Nanomaterials. *Chem. Soc. Rev.* **2016**, *45*, 1750−1780.
(67) Naumkin, A. V.; Kraut-Vass, A.; Gaarenstroom, S. W.; Powell, C. J. *NIST X-ray Photoelectron Spectroscopy (XPS) Database*; Version 4.1. http://srdata.nist.gov/xps 2012.
(68) Choi, J.-G.; Thompson, L. T. XPS Study of As-Prepared and Reduced Molybdenum Oxides. *Appl. Surf. Sci.* **1996**, *93*, 143−149.
(69) Martín-Luengo, A. T.; Köstenbauer, H.; Winkler, J.; Bonanni, A. Processing and Charge State Engineering of MoO_x. *AIP Adv.* **2017**, *7*, No. 015034.
(70) Cherevko, S.; Topalov, A. A.; Zeradjanin, A. R.; Katsounaros, I.; Mayrhofer, K. J. J. Gold Dissolution: Towards Understanding of Noble Metal Corrosion. *RSC Adv* **2013**, *3*, 16516−16527.

https://dx.doi.org/10.1021/acsami.0c06198
ACS Appl. Mater. Interfaces 2020, 12, 25200−25210